

All Vehicles Can Lie: Efficient Adversarial Defense in Fully Untrusted-Vehicle Collaborative Perception via Pseudo-Random Bayesian Inference

Yi Yu¹, Libing Wu^{1†}, Zhuangzhuang Zhang¹, Jing Qiu², Lijuan Huo¹, Jiaqi Feng¹

¹School of Cyber Science and Engineering, Wuhan University

²Cyberspace Institute of Advanced Technology, Guangzhou University

{yui1212, wu, zhzhuangzhuang, lijuanHuo, jiaqiFeng}@whu.edu.cn, qiuqing@gzhu.edu.cn

Abstract

Collaborative perception (CP) enables multiple vehicles to augment their individual perception capacities through the exchange of feature-level sensory data. However, this fusion mechanism is inherently vulnerable to adversarial attacks, especially in fully untrusted-vehicle environments. Existing defense approaches often assume a trusted ego vehicle as a reference or incorporate additional binary classifiers. These assumptions limit their practicality in real-world deployments due to the questionable trustworthiness of ego vehicles, the requirement for real-time detection, and the need for generalizability across diverse scenarios. To address these challenges, we propose a novel Pseudo-Random Bayesian Inference (PRBI) framework, a first efficient defense method tailored for fully untrusted-vehicle CP. PRBI detects adversarial behavior by leveraging temporal perceptual discrepancies, using the reliable perception from the preceding frame as a dynamic reference. Additionally, it employs a pseudo-random grouping strategy that requires only two verifications per frame, while applying Bayesian inference to estimate both the number and identities of malicious vehicles. Theoretical analysis has proven the convergence and stability of the proposed PRBI framework. Extensive experiments show that PRBI requires only 2.5 verifications per frame on average, outperforming existing methods significantly, and restores detection precision to between 79.4% and 86.9% of pre-attack levels.

1. Introduction

Multi-vehicle collaborative perception (CP) enables connected and autonomous vehicles (CAVs) to extend their perceptual range by sharing sensor data via vehicle-to-vehicle (V2V) communication [5, 6]. This mitigates blind spots inherent to single-vehicle sensing. Generally, CP can be implemented through raw data-level (early), feature-level

(intermediate), or decision-level (late) fusion, with intermediate fusion offering the best trade-off between efficiency and accuracy [10, 18, 29]. However, it also exposes the ego vehicle to increased security risks. Malicious collaborators can inject adversarial perturbations into shared feature maps, causing substantial perception errors when fused by the ego vehicle [27]. Effective defense thus hinges on detecting and isolating such malicious vehicles.

Sampling-based defenses [9, 16] have been proposed to mitigate adversarial threats in CP. These methods typically validate information consistency between the ego vehicle and sampled collaborators via iterative consensus algorithms. Although demonstrating robustness against specific attack patterns, their effectiveness fundamentally depends on two strong assumptions: (1) the absolute reliability of ego vehicle inputs, and (2) prior knowledge of attacker conditions. Such requirements significantly constrain their operational adaptability and computational efficiency. In addition, classifier-based approaches [8, 25, 37] train binary classifiers to distinguish malicious collaborators from benign ones based on statistical patterns such as feature residual distributions between benign (ego) and malicious vehicles. While offering greater flexibility, these methods expand the attack surface, struggle to generalize to unseen scenarios, and impose significant computational overhead, thereby posing substantial challenges to practical deployment. Accordingly, this paper focuses on sampling-based validation as a more robust and lightweight alternative.

However, a fundamental limitation common to all existing methods is the assumption that the ego vehicle is inherently trustworthy and its perception results can serve as a reliable reference. In reality, non-ego vehicles can be directly manipulated by attackers, who inject adversarial perturbations into their feature maps and subsequently transmit the tampered data to the ego vehicle. For the ego vehicle, although attackers cannot directly compromise its internal system, they can still disrupt its feature map via LiDAR injection attacks [11, 23] or data interception attacks [3]. Thus, this assumption is misaligned with real-world scenar-

† Corresponding author.

ios, where the CP environment is a fully untrusted-vehicle setting and all vehicles (including the ego one) must be treated as potentially malicious entities capable of transmitting adversarial features [19, 31, 36]. In short, *All Vehicles Can Lie* in realistic scenarios. This significantly complicates the task of detecting malicious feature maps within the ego vehicle. Moreover, the verification count per frame for both sampling- and classifier-based approaches increases linearly with the total number of vehicles, leading to a low detection efficiency. In summary, achieving **robust adversarial defense** with **minimal verification cost** remains a critical challenge in CP, where *all vehicles can lie*.

To tackle this, it is essential to first establish a realistic and robust reference signal. Inspired by the inherent spatial continuity between adjacent frames [1, 17], we hypothesize that LiDAR-based perception outputs across successive frames also exhibit a consistent degree of similarity that exceeds a critical threshold. To verify this hypothesis, we compute the Jaccard similarity [22] between perception outputs across consecutive frames under various normal and adversarial settings (see appendix for experimental details). Extensive evaluations show that inter-frame similarity is stably around 0.8 in benign scenarios, whereas adversarial settings cause it to drop sharply. This pronounced and consistent gap confirms that temporal consistency can serve as a reliable self-referential signal even without assuming any trusted vehicle, enabling us to replace the ego-trust assumption with a frame-wise self-supervision mechanism that uses the prior frame as a probabilistic reference.

Building on the validated hypothesis, we propose the novel **Pseudo-Random Bayesian Inference (PRBI)** defense framework, a mathematically principled method for efficient and assumption-free detection of malicious vehicles in fully untrusted-vehicle CP without prior knowledge of attackers. Specifically, we design a **pseudo-random grouping strategy** that requires only two additional verifications per frame, completely decoupling the number of verifications from the total number of vehicles and significantly reducing detection costs. Additionally, we mathematically model this grouping strategy as a repeated random sampling process, estimating the number of malicious vehicles through mathematical approximation and evaluating the benign probability of each vehicle using **Bayesian probabilistic inference**. By combining the estimated number of malicious vehicles with the benign probability of individual cars, suspected malicious vehicles can be identified and filtered out. To further enhance detection efficiency, we incorporate **hypothesis testing** techniques, enabling PRBI to preemptively assess convergence and prioritize the fusion of features from vehicles deemed trustworthy during the non-convergence stage. Meanwhile, we rigorously validate the PRBI framework through formal mathematical proofs of its convergence and rounding operation properties, thereby es-

tablishing its theoretical guarantees for attacker detection.

Our main contributions are as follows:

- We analyze inter-frame perceptual similarity and **first** exploit it as a self-referential defense signal for **fully untrusted-vehicle** CP, which addresses the core challenge when *all vehicles can lie*.
- We propose the **Pseudo-Random Bayesian Inference (PRBI)** framework, achieving robust fusion and attacker detection without prior knowledge, averaging only two verifications per frame.
- We theoretically prove PRBI’s convergence and validity from **a mathematical perspective** and conduct a comprehensive evaluation to demonstrate its effectiveness.

2. Related Work

Adversarial CP. Recent studies reveal that CP is more susceptible to adversarial attacks than single-agent systems [24, 26, 28, 32, 34]. In feature-level fusion, attackers can embed malicious perturbations into shared feature maps via white-box methods (e.g., PGD, C&W) [27, 35], severely degrading perception accuracy. Existing defenses such as adversarial training [21] suffer from limited generalization and high computational costs, while detection-based approaches [8, 25, 37] struggle against adaptive attacks.

Defensive CP. Defense strategies can be broadly categorized into sampling-based and classifier-based approaches. Sampling-based methods [9, 16, 35] enforce consistency between the ego vehicle and a subset of collaborators via iterative consensus protocols. While offering partial robustness, they rely on strong trust assumptions and adversarial priors, limiting applicability in fully untrusted environments. Classifier-based defenses [8, 25, 37] detect malicious participants by learning discriminative patterns in residuals between shared and local features; however, their performance degrades when multiple vehicles are compromised or under diverse driving conditions. Recent work on security-aware sensor fusion further explores probabilistic trust modeling. MATE [7] proposes a geometry-based multi-agent trust estimator that updates trust scores according to observation consistency, requiring object tracking and visibility reasoning. In contrast, PRBI is geometry-free and leverages self-referential temporal consistency across pseudo-random collaborator subsets, enabling attack detection without explicit scene modeling, tracking, or ego-trust assumptions. By removing prior trust requirements and attacker assumptions, PRBI provides mathematically grounded robustness with constant detection overhead.

3. Attack Formulation

3.1. Attack Model

We focus on a vehicle-to-vehicle (V2V) collaborative perception (CP) scenario, as shown in Fig. 1. Similar to previ-

ous defensive work, we assume that all vehicles employ the same LiDAR-based feature-level CP model, and any feature map may be perturbed. Before an attack, the attacker selects a fixed set of malicious vehicles (including the ego vehicle), constrained by the limited budget to compromise all participants. During an attack frame, all malicious vehicles are controlled to produce adversarial features. Perception errors arise when the ego fuses these corrupted features with its own. The defense objective is thus to detect and exclude malicious feature contributions before fusion.

3.2. Problem Formulation

We consider a collaborative scenario involving n CAVs, denoted as a_1, a_2, \dots, a_n , where a_1 represents the ego vehicle and $n \geq 2$. Each vehicle is equipped with the same feature encoder $f_{\mathcal{E}}(\cdot)$, feature fusion module $f_{\mathcal{F}}(\cdot)$, and object detection decoder $f_{\mathcal{D}}(\cdot)$. At time frame t , vehicle a_i captures LiDAR point cloud raw data C_i^t , which is encoded into a feature map: $F_i^t = f_{\mathcal{E}}(C_i^t) \in \mathbb{R}^{W \times H \times C}$, where W , H , and C denote the width, height, and number of channels of the feature map, respectively. Vehicles broadcast their encoded features to collaborators. Upon reception, a_i transforms received maps into its local coordinate frame via $f_{\mathcal{T}}(\cdot)$ and fuses them with its own: $H_i^t = f_{\mathcal{F}}(F_i^t \cup f_{\mathcal{T}}(\{F_j^t\}_{j \neq i}))$. The fused representation is then decoded to yield perception outputs $D_i^t = f_{\mathcal{D}}(H_i^t) = \{d_j\}_{j \in [1, L]}$, where L is the number of predicted bounding boxes, each $d_j \in \mathbb{R}^{c+l}$ containing c class logits and l location parameters.

Adversarial Perception. In a fully untrusted-vehicle setting, the victim’s own feature map may also be compromised without its awareness. The adversary arbitrarily compromises k out of n vehicles, $1 \leq k \leq n - 1$, forming the malicious set M . The attack aims to mislead the ego’s perception by injecting bounded perturbations $\delta \in \mathbb{R}^{W \times H \times C}$ into the feature maps $\{F_i^t\}_{i \in M}$, with the dual objectives of concealing real targets and inducing false object perceptions. After fusion, the ego’s perception output becomes:

$$D_1^t(\delta) = f_{\mathcal{D}} \circ f_{\mathcal{F}} \circ f_{\mathcal{T}}(\{F_i^t + \delta\}_{i \in M} \cup \{F_j^t\}_{j \notin M}) = \{d_j'\}_{j \in [1, L]}. \quad (1)$$

The perturbation is bounded by $\|\delta\| \leq \Delta$ and optimized to maximize divergence as follows:

$$\max_{\|\delta\| \leq \Delta} \sum_{j=1}^L \mathcal{L}_{\text{det}}(d_j, d_j'), \quad (2)$$

where \mathcal{L}_{det} is the multi-agent standard detection loss following [27, 37] and Δ constrains perturbation magnitude.

4. PRBI Defense Method

4.1. Defense Challenges and Key Findings

In fully untrusted-vehicle CP scenarios, designing an effective defense faces three key challenges: **C1: Detection**

Table 1. Comparison between the theoretical probability of sampling an all-benign group and the empirical probability obtained by randomly splitting vehicles into two groups. The frame count is recorded once the observed probability η converges to P'_{ideal} .

Attacker Number ($n = 5$)	1	2	3	4
Theoretical Prob. P_{ideal}	0.484	0.226	0.097	0.032
Approximate Prob. P'_{ideal}	0.500	0.250	0.125	0.063
Validation Frame Count	40	29	28	21
Practical All-Benign Prob. η	0.491	0.258	0.103	0.045

without trust assumptions. The defender has no prior knowledge of which vehicles are malicious, their number or proportion, and even the ego vehicle may be compromised, making it difficult to detect attackers without any trust assumption. **C2: Scalability of per-frame defense cost.** Existing sampling or verification methods incur per-frame costs that grow linearly with fleet size, which is impractical for real-time large-scale CP. Achieving constant-cost detection per frame is essential. **C3: Fast and complete attacker identification.** Randomized sampling may delay attacker exclusion, causing prolonged risk exposure. The third key challenge is to guarantee both high detection speed and completeness despite sampling randomness.

To tackle these challenges, we derive two key findings: **F1: Inter-frame similarity divergence enables ego-agnostic detection.** To address **C1**, we conduct a dedicated experiment analyzing the similarity of perception results between consecutive frames and obtain the following key observation: benign perception exhibits significantly higher inter-frame similarity compared to adversarial perception (see the appendix for details). We conclude that benign perception maintains an average similarity of around 0.8, while adversarial cases rarely exceed 0.3. This property allows using the previous frame’s verified benign output as a trusted reference for current-frame detection, removing dependency on prior trust assumptions. **F2: Binary grouping approximates random sampling and implicitly encodes key information about malicious vehicles.** Theoretically, the minimum cost for additional verification per frame is two verifications. To approach this optimal cost, we divide all vehicles into two random groups per frame and validate each group’s collaborative perception result against the benign perception of the previous frame. This yields two key insights: (1) *Binary grouping statistically resembles random sampling without replacement*, where the probability of obtaining an all-benign group is:

$$P_{ideal} = \frac{2^{n-k} - 1}{2^n - 1} \approx P'_{ideal} = \frac{2^{n-k}}{2^n}. \quad (3)$$

The experiments shown in Tab. 1 confirm that in finite frames, binary grouping closely approximates this process ($\eta \approx P'_{ideal}$), with P'_{ideal} providing a tractable estimate dependent only on the attacker number k . (2) *Binary group*

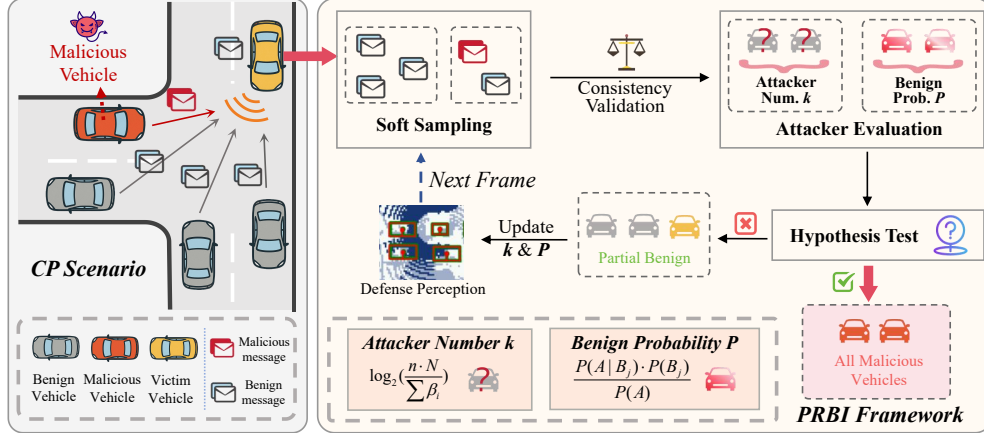


Figure 1. The Pseudo-Random Bayesian Inference (PRBI) framework methodology overview.

verification reveals per-vehicle trustworthiness. Each group verification yields not only a group-level result but also a single validation outcome per participating vehicle. By maintaining two counters per vehicle (one for successful benign and one for failed malicious validations), we track every vehicle’s verification history. The global empirical benign ratio η of normal validations can then be computed using the verification history and approximated to P'_{ideal} . From this, we can infer the number of attackers as follows:

$$k = \log_2\left(\frac{1}{P'_{ideal}}\right) \approx \log_2\left(\frac{1}{\eta}\right). \quad (4)$$

Furthermore, a vehicle involved in almost no benign verifications is likely to be malicious. Thus, by combining the estimated k and per-vehicle validation statistics, we can identify likely attackers. In conclusion, binary grouping not only addresses the core of **C2** but also enables efficient, cost-effective defense which is essential for **C3**.

4.2. PRBI Overview

As observed in **F1**, the distribution of perception bounding box similarity between adjacent frames differs significantly under normal versus adversarial conditions. We quantify this using Jaccard similarity, defined for two consecutive detection sets D^t and D^{t-1} as:

$$\text{Jaccard}(D^t, D^{t-1}) = \frac{|\mathcal{M}|}{|D^t| + |D^{t-1}| - |\mathcal{M}|}, \quad (5)$$

where \mathcal{M} is the set of matched pairs (Hungarian matching with IoU above a threshold [12]) and $|\mathcal{M}|$ denotes the number of valid matches. Leveraging this distributional gap, we assume the initial frame’s perception is entirely correct. For subsequent frames, if the similarity with the previous frame falls below a warning threshold ϵ , the frame is flagged as potentially attacked. Then, building upon **F2**, PRBI detects and excludes malicious vehicles through following steps:

- **Step 1: Initialization.** At $t = 0$, initialize two n -dimensional arrays: normal detection counts $\mathbf{c}_{normal} = (\beta_1, \dots, \beta_n)$ and abnormal detection counts $\mathbf{c}_{abnormal} = (N - \beta_1, \dots, N - \beta_n)$, with N (total detections) and β_i set to 0, n represents the total number of vehicles.
- **Step 2: Soft Sampling & Consistency Validation.** For each frame, the victim vehicle partitions received shared features into two groups using **soft sampling** strategy, performs perception fusion, and computes similarity with the previous benign frame. Groups exceeding ϵ have their members’ β_i incremented. Then N and both count arrays (\mathbf{c}_{normal} , $\mathbf{c}_{abnormal}$) are updated.
- **Step 3: Attacker Evaluation.** Using \mathbf{c}_{normal} and $\mathbf{c}_{abnormal}$, apply probabilistic approximation and Bayesian probabilistic inference to estimate the number of suspicious malicious vehicles m and each vehicle’s benign probability $P_{benign} = (p_1, \dots, p_n)$. Meanwhile, select the m vehicles with the lowest benign probabilities as the estimated malicious vehicles, thus addressing **C1** and **C2**.
- **Step 4: Hypothesis Testing & Defense Perception.** A T-test is applied to determine if estimates have converged (addressing **C3**). If converged, the attacker set $M = \{\text{argsort}(P_{benign})_{0:[m]}\}$ and count m are output; otherwise, vehicles with $p_i \neq 0$ serve as collaborators in the next frame and return to step 2. Since $\beta_i = 0$ for any true attacker, its p_i remains zero, ensuring eventual exclusion. More details are provided in Sec. 4.3.

The convergence of m to the true number of attackers k is critical to the effectiveness of PRBI, and the corresponding theorems are provided in Sec. 5.

4.3. PRBI Framework Design

Given reference perception D_{ref} from the previous benign frame, PRBI executes four core steps: (i) soft sampling via pseudo-random grouping, (ii) group consistency validation, (iii) attacker estimation, and (iv) convergence testing. The pseudocode of PRBI is provided in the appendix.

Soft Sampling. To minimize verification costs, we propose a pseudo-random grouping based on **F2**. This strategy divides all shared information into two groups and performs only two additional verifications per frame. Specifically, at each frame, we divide the most suspicious $\lfloor m \rfloor$ vehicles into one group and the rest into the second group to approximate the random sampling process:

$$(Group_1, Group_2) = (\pi_{0:\lfloor m \rfloor}, \pi_{\lfloor m \rfloor:n}), \quad (6)$$

where $\pi = \text{argsort}(P_{\text{benign}})$ and m is the current estimated number of attackers. This method has two main advantages: First, by simulating the sampling-without-replacement process, it can effectively uncover hidden information (see **F2**). Second, the pseudo-random grouping strategy based on m and P_{benign} ensures that the final estimated number of attackers m converges to the actual number k . Additionally, to guarantee convergence, m must be floored, and other rounding operations may cause convergence bias. A detailed proof of these conclusions is provided in Sec. 5.

Consistency Validation. Based on the previous frame's reliable perception results D_{ref} , the two groups are sequentially subjected to consistency validation. For each group, feature-level collaborative perception is first performed, and its consistency with the reference result is then computed as $\text{Jaccard}(D_{\text{Group}}, D_{\text{ref}})$. If the consistency value exceeds the threshold ϵ , it indicates that the group likely contains no malicious vehicles, and the normal detection count for each vehicle in the group $\{\beta_i | i \in \text{Group}\}$ is incremented by 1. After both groups are validated, the total number of detections N for each vehicle is increased by 1, and the arrays $\mathbf{c}_{\text{normal}}$ and $\mathbf{c}_{\text{abnormal}}$ are updated in sequence. In other words, the consistency validation results are used to maintain the updates of $\mathbf{c}_{\text{normal}}$ and $\mathbf{c}_{\text{abnormal}}$, which are critical for the subsequent evaluation of potential attackers.

Attacker Evaluation. We first estimate the number of attackers. Assuming that in each round, a group of vehicles is randomly sampled from all vehicles, and based on the idealized random process (see Eq. (3)), the probability ρ of sampling an all-benign group can be expressed as:

$$\rho = \frac{2^{n-k} - 1}{2^n - 1} \approx \frac{2^{n-k}}{2^n} = 2^{-k}, \quad (7)$$

where n denotes the total number of vehicles and k is the true number of attackers. Meanwhile, using $\mathbf{c}_{\text{normal}}$ and $\mathbf{c}_{\text{abnormal}}$, the empirical ratio η of normal detection counts can be calculated as:

$$\eta = \frac{\text{Benign Counts}}{\text{Total Counts}} = \frac{\sum \mathbf{c}_{\text{normal}}}{\sum_{i=1}^n N} = \frac{\sum_{i=1}^n \beta_i}{n \cdot N}. \quad (8)$$

Through **F2** in Sec. 4.1, we can approximate η to ρ and estimate the number of attackers like Eq. (4). Thus, we assume $\eta \approx \rho$, and the number of attackers can be estimated as:

$$m = \log_2 \left(\frac{1}{\rho} \right) \approx \log_2 \left(\frac{1}{\eta} \right) = \log_2 \left(\frac{n \cdot N}{\sum_{i=1}^n \beta_i} \right). \quad (9)$$

After estimating the number of attackers, the next step is to identify specific malicious vehicles by computing the *benign probability* $P_{\text{benign}}[j]$ of each vehicle based on Bayes' theorem. Let \mathcal{A} denote the event that an attack occurs and \mathcal{B}_j the event that vehicle j is benign. According to Bayes' rule, the posterior benign probability is given by:

$$P_{\text{benign}}[j] = P(\mathcal{B}_j | \mathcal{A}) = \frac{P(\mathcal{A} | \mathcal{B}_j) \cdot P(\mathcal{B}_j)}{P(\mathcal{A})}. \quad (10)$$

Here, $P(\mathcal{A} | \mathcal{B}_j)$ represents the likelihood of observing an attack given that vehicle j is benign, which is estimated as:

$$P(\mathcal{A} | \mathcal{B}_j) = \frac{\sum \mathbf{c}_{\text{abnormal}} - \mathbf{c}_{\text{abnormal}}[j]}{\sum_{i=1}^n N - N}. \quad (11)$$

The prior benign probability $P(\mathcal{B}_j)$ is defined as a weighted sum of the short-term benign probability from the previous frame and the long-term normal detection ratio:

$$P(\mathcal{B}_j) = \gamma \cdot P_{\text{benign}}[j] + \lambda \cdot \frac{\mathbf{c}_{\text{normal}}[j]}{N}, \quad (12)$$

where P_{benign} is initialized to $\mathbf{0}$ at first frame, and γ and λ are the respective weights for short-term and long-term components. This design mitigates the influence of early unstable groupings by incorporating temporal memory. Finally, the global probability of an attack $P(\mathcal{A})$ is given by the proportion of abnormal detections in the entire system $P(\mathcal{A}) = \frac{\sum \mathbf{c}_{\text{abnormal}}}{\sum_{i=1}^n N}$. Based on the estimated number of attackers m , the set of suspected malicious vehicles consists of the $\lfloor m \rfloor$ vehicles with the lowest benign probabilities:

$$\text{Attackers} = \text{argsort}(P_{\text{benign}})_{0:\lfloor m \rfloor}. \quad (13)$$

Hypothesis Testing. By iteratively executing the above steps, the estimated attacker number m eventually converges to the true attacker count k , and the set *Attacker* is guaranteed to include all malicious vehicles (see mathematical theorem in Sec. 5). To eliminate redundant group verification, PRBI determines whether m has converged using the hypothesis testing method in advance. The reason for using hypothesis testing is that we observe that m fluctuates within a small range around k , and when this fluctuation remains confined within a certain interval for many frames, it can be considered as convergence. Hypothesis testing is well-suited for this. Specifically, we maintain a queue W of window size w , storing the estimated m values from the past w_p frames as sample data ($w_p \leq w$, w_p is as large as possible). Then, in the current frame, we define the null hypothesis $H_0 : k = m$ and the alternative hypothesis $H_1 : k \neq m$. The sample mean is $\bar{x} = \frac{1}{w_p} \sum_{i=1}^{w_p} W_i$, and the sample variance is $S^2 = \frac{1}{w_p - 1} \sum_{i=1}^{w_p} (W_i - \bar{x})^2$. Next, we perform a T-test with confidence level α to compute the rejection region \mathcal{W} and test H_0 :

$$\mathcal{W} = \left\{ \left| \frac{\bar{x} - m}{S / \sqrt{w_p}} \right| > t_{\frac{\alpha}{2}}(w_p - 1) \right\}, \quad (14)$$

where $t_{\frac{\alpha}{2}}(w_p - 1)$ denotes the upper quantile of the t-distribution with $w_p - 1$ degrees of freedom. To prevent the slow convergence of m from falsely causing the T-test to accept H_0 , we introduce a second convergence condition. For a malicious vehicle j , the number of normal detections β_j must be 0. Hence, both $P(\mathcal{B}_j)$ and $P_{\text{benign}}[j]$ must also be 0 (as derived from Eq. (12) and Eq. (10)). When m converges, its value must equal the number of vehicles with zero benign probability in P_{benign} . This forms the second convergence condition. When both conditions are satisfied, the current *Attacker* set is exactly the set of all malicious vehicles, indicating a successful detection. If the convergence conditions are not met, then we select vehicles with non-zero benign probability as collaborators for this frame to perform perception (according to the second convergence condition), and use their benign perception results to update the reference for the next frame’s detection process.

When abnormal frames first appear, both sampled groups may contain malicious vehicles, resulting in all vehicles having zero benign probability. To select valid collaborators in this frame, the divide-and-conquer method is used to recursively search for the first valid subset of benign vehicles in the two groups to serve as collaborators for the current frame, while also updating $\mathbf{c}_{\text{normal}}$, N , and $\mathbf{c}_{\text{abnormal}}$.

5. Theoretical Results

In this section, we present our main theoretical conclusions about the convergence of the estimated attacker number m under the proposed **pseudo-random grouping** strategy, as well as the effect of different rounding schemes. The complete proofs are provided in the appendix.

Theorem 1 (Convergence of m to k). *Under the pseudo-random grouping strategy, the estimated number of attackers m will monotonically converge to the true number of attackers k .*

Theorem 2 (Effect of Rounding Strategy). *Let $\lfloor \cdot \rfloor$, $\lceil \cdot \rceil$, and $\lceil \cdot \rceil$ denote floor, ceiling, and nearest-integer rounding. Only the floor rounding $\lfloor m \rfloor$ guarantees the exact convergence of m to k under pseudo-random grouping. The nearest-integer and ceiling rounding result in convergence to $k - 0.5$ and $k - 1$, respectively. Note that when the true number of attackers $k = 1$ with ceiling rounding, m will not tend toward 0. In this case, the final m will converge to $\log_2(\frac{n}{n-1})$.*

6. Experiments

6.1. Experimental Setups

We evaluate PRBI on the V2X-Sim dataset [15], which provides multi-vehicle LiDAR point clouds in the nuScenes format [2]. Detection performance is measured by Average Precision (AP) at IoU thresholds of 0.5 and 0.7, while efficiency is quantified by the number of additional verification

Table 2. Comparison of the verification count per frame. The best results are marked in blue. PRBI yields the lowest detection cost.

Methods	Metric ↓	Attacker Ratio (%)				Avg. ↓
		20	40	60	80	
ROBOSAC [16]	Min	1	1	1	1	1.0
	Max	19	39	46	17	30.3
	Avg	4.89	10.36	8.29	4.73	7.1
PASAC [9]	Min	4	4	6	8	5.5
	Max	6	8	8	8	7.5
	Avg	4.79	6.60	7.59	8.00	6.7
PRBI (Ours)	Min	2	2	2	2	2.0
	Max	2	4	6	8	5.0
	Avg	2.00	2.35	2.61	2.86	2.5

comparisons per frame. For adversarial settings, we adopt BIM [13], C&W [4], and PGD [21]. The collaborative perception framework is based on V2VNet [30] for feature fusion and FaFNet [20] as the detection backbone. To assess the robustness of PRBI under different fusion paradigms, we also compare simple fusion strategies (mean, max, and sum) with the advanced DiscoNet [14]. The single-vehicle lower-bound baseline follows the feature mean fusion setting [33]. We further compare PRBI with the SOTA defenses: ROBOSAC [16] and PASAC [9].

6.2. Defense Effectiveness

Comparison with Counterparts. Tab. 2 reports the verification cost per frame for $n = 5$ under varying attacker ratios. PRBI achieves the lowest average cost (2.5 verifications per frame) and remains stable between 2 and 3 across all attack intensities, demonstrating strong robustness to adversarial variation. When both groups contain attackers in the first abnormal frame, PRBI employs a divide-and-conquer query strategy. Although this may slightly increase the peak cost, the search terminates once a benign subset is found, incurring minimal delay. Overall, the maximum verification count of PRBI averages 5.0, significantly lower than ROBOSAC (30.3) and PASAC (7.5).

Detection Defense Performance. Tab. 3 summarizes results under different settings for $n = 5$ and $k = 2$. Under the V2VNet backbone, PRBI effectively restores performance, recovering 79.4%, 81.0%, and 86.9% of AP loss against PGD, BIM, and C&W, respectively. The defended results consistently exceed the Lower-Bound and approach the benign Upper-Bound. Moreover, PRBI maintains stable robustness across diverse fusion paradigms, achieving comparable recovery levels under all settings. Compared with SOTA, PRBI achieves 1.3–3.5% higher AP than ROBOSAC and 1.0–4.0% higher than PASAC. Visualization in Fig. 2 further illustrate that PRBI successfully filters out adversarial vehicles and preserves accurate perception.

Varying Test Parameters. We evaluate the impact of the confidence level α and window size w in the T-test on PRBI’s detection efficiency and accuracy, as summarized

Table 3. Detection performance when $n = 5$ and $k = 2$ under different fusion strategies. *Lower-Bound* denotes single-vehicle perception, while *Upper-Bound* represents collaborative perception without attacks. ‘ w ’ indicates ‘with’. Best results are marked in blue, and comparisons with baseline methods demonstrate the average defense performance across test datasets.

Methods	Mean Fusion		Max Fusion		Sum Fusion		V2VNet [30]		DiscoNet [14]	
	AP@0.5↑	AP@0.7↑								
Upper-Bound	79.57	75.34	78.62	75.07	77.88	74.38	80.73	78.35	80.52	76.72
Attack w PGD	16.51	14.60	27.16	26.45	13.65	7.31	17.02	14.53	20.97	19.54
PRBI against PGD	65.36 ^{+48.85}	61.44 ^{+46.84}	64.89 ^{+37.73}	62.02 ^{+35.57}	70.78 ^{+57.13}	67.67 ^{+60.36}	68.93 ^{+51.91}	63.82 ^{+49.29}	69.18 ^{+48.21}	65.68 ^{+46.14}
Attack w BIM	13.67	9.08	33.54	32.71	4.56	4.13	13.51	11.69	21.02	18.53
PRBI against BIM	66.37 ^{+52.70}	60.72 ^{+51.64}	65.87 ^{+32.33}	63.30 ^{+30.59}	70.81 ^{+66.25}	67.65 ^{+63.52}	68.76 ^{+55.25}	64.88 ^{+53.19}	66.17 ^{+45.15}	63.27 ^{+44.74}
Attack w C&W	7.51	3.42	25.99	24.88	8.52	7.12	10.68	6.04	14.90	10.93
PRBI against C&W	70.58 ^{+63.07}	68.49 ^{+65.07}	66.59 ^{+40.60}	61.91 ^{+37.03}	74.13 ^{+65.61}	71.16 ^{+64.04}	71.87 ^{+61.19}	68.54 ^{+62.50}	72.98 ^{+58.08}	69.06 ^{+58.13}
Lower-Bound	56.35	52.89	56.35	52.89	56.35	52.89	56.35	52.89	56.35	52.89
ROBOSAC [16]	66.17 ^{+9.82}	63.05 ^{+10.16}	63.58 ^{+7.23}	57.36 ^{+4.46}	64.07 ^{+7.72}	59.61 ^{+6.72}	64.13 ^{+7.78}	61.01 ^{+8.12}	65.29 ^{+8.94}	63.87 ^{+10.98}
PASAC [9]	64.38 ^{+8.03}	60.07 ^{+7.18}	65.96 ^{+9.61}	62.29 ^{+9.40}	67.98 ^{+11.63}	63.60 ^{+10.71}	68.39 ^{+12.04}	64.73 ^{+11.83}	69.08 ^{+12.73}	64.54 ^{+11.65}
PRBI (Ours)	67.44 ^{+11.09}	63.55 ^{+10.66}	65.78 ^{+9.43}	62.41 ^{+9.52}	71.91 ^{+15.56}	68.83 ^{+15.94}	69.85 ^{+13.50}	65.75 ^{+12.86}	69.44 ^{+13.09}	66.00 ^{+13.11}

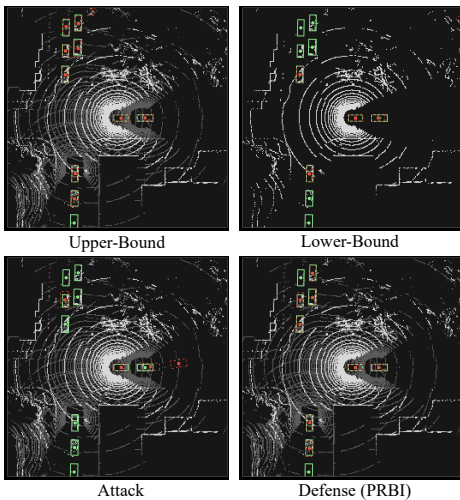


Figure 2. Visualization of defense performance with green boxes for ground truth and red boxes for predictions.

in Tab. 4. Specifically, we record the *Average Convergence Frames*, the *Identification Rate* of malicious vehicles, and the *Misclassification Rate* of benign ones. Results show that PRBI converges within approximately *four* frames on average while maintaining a 100% identification rate for malicious vehicles. When the attacker ratio reaches 0.4, a slight performance drop (6% misclassification) occurs because the test statistic m stabilizes prematurely before all benign samples are included, causing the T-test to signal early convergence and misclassify one benign vehicle as malicious. Nevertheless, the malicious identification rate consistently remains 100%. Moreover, sensitivity analysis on α and w further supports this observation: reducing α accelerates convergence (frames decrease from 3.99 to 3.36) without degrading accuracy, while larger w yields smoother convergence. Overall, PRBI demonstrates a robust balance between efficiency and reliability across all tested configu-

Table 4. Impact of different test parameters on defense effect. *Min/Max*: verification count range. *Avg. Min/Max*: average verification counts. *Avg.*: overall average count. *Avg. Frames*: average frames to convergence. *ID Rate*: malicious vehicle identification rate. *MC Rate*: benign vehicle misclassification rate.

Settings	Count		Avg. Count		Avg.	Avg. Frames	ID Rate	MC Rate
	Min	Max	Min	Max				
Attacker Ratio								
Ratio 80%	2	8	2.00	5.70	2.86	4.27	100%	0%
Ratio 60%	2	6	2.00	4.06	2.61	3.36	100%	0%
Ratio 40%	2	4	2.00	2.88	2.35	2.77	100%	6%
Ratio 20%	2	2	2.00	2.00	2.00	2.25	100%	0%
Confidence Level (60% Attackers)								
Conf. 0.20	2	6	2.00	4.22	2.61	3.99	100%	0%
Conf. 0.15	2	6	2.00	4.12	2.62	3.51	100%	0%
Conf. 0.10	2	6	2.00	3.94	2.53	3.44	100%	0%
Conf. 0.05	2	6	2.00	4.26	2.67	3.40	100%	0%
Conf. 0.01	2	6	2.00	4.06	2.61	3.36	100%	0%
Window Size (80% Attackers)								
Size 10	2	8	2.00	5.70	2.86	4.27	100%	0%
Size 8	2	8	2.00	6.16	2.91	4.60	100%	0%
Size 6	2	8	2.00	6.10	2.89	4.57	100%	0%
Size 4	2	8	2.00	6.34	2.88	4.89	100%	0%

rations. Detailed results are presented in the appendix.

6.3. Algorithm Convergence

To intuitively verify the convergence of PRBI (Sec. 5), we record the evolution of m under three rounding strategies with six vehicles and plot the results in Fig. 3. When using floor rounding, m consistently converges to the true attacker count k , in line with Theorem 1. For rounding-to-nearest and ceiling modes, m converges to $k - 0.5$ and $k - 1$, respectively. Notably, when $k = 1$, the ceiling mode yields $m \approx \log_2(n/(n-1)) \approx 0.263$, perfectly matching the theo-

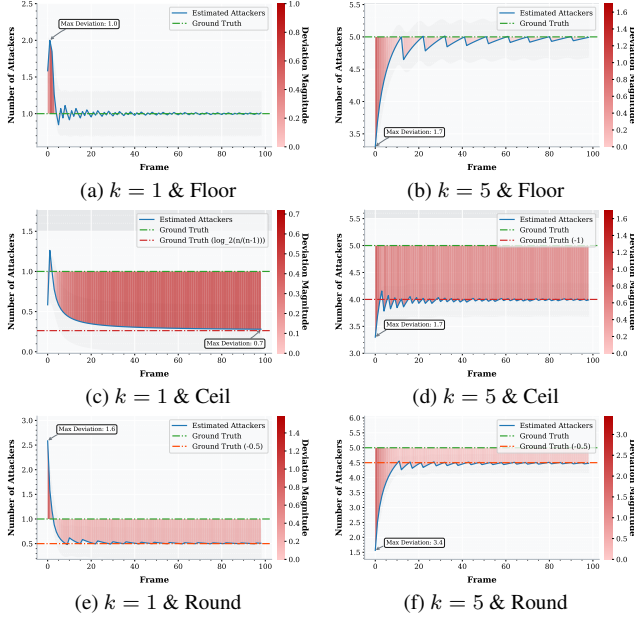


Figure 3. Convergence behavior of m with total 6 vehicles under different rounding strategies. The blue solid line denotes the value of m calculated using Eq. (9), the green dashed line marks the true number of attackers k , and the red dashed line represents the theoretically derived convergence value in Theorem 2.

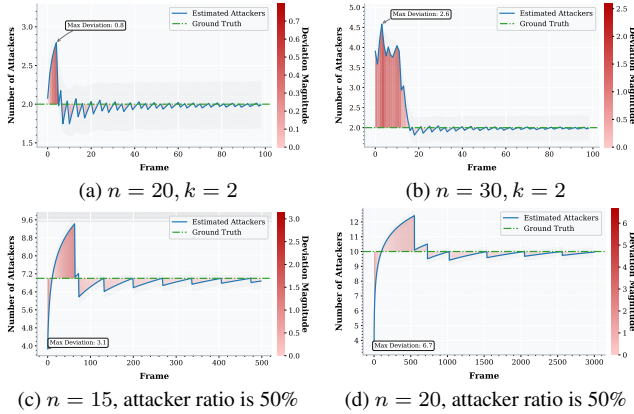


Figure 4. The convergence characteristics of PRBI's frame-by-frame estimation of the calculated malicious vehicles number m .

retical result in Theorem 2. Across all settings, the deviation between estimated m and k never exceeds 2, confirming the numerical stability induced by the logarithmic form.

To further analyze convergence behavior, we examine two scenarios with varying vehicle counts. In Figs. 4a and 4b, with a fixed number of attackers, larger n slows convergence since a greater denominator increment is needed in Eq. (9) to satisfy the logarithmic condition. When the attacker ratio is fixed, both n and k increase, causing the logarithmic term to grow rapidly and convergence to slow down. As illustrated in Figs. 4c and 4d, convergence takes about 100 frames for $n = 15$ and up to 500 frames for $n = 20$.

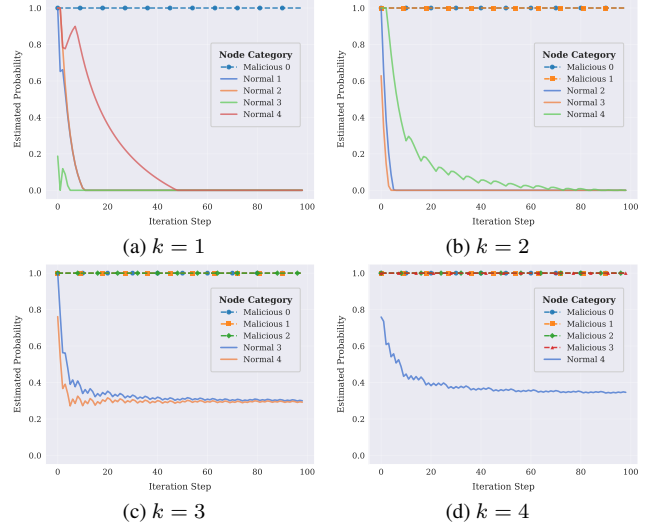


Figure 5. The probability of malicious behavior for all vehicles under varying numbers of attackers.

6.4. Probability Trend of Vehicles

To analyze how the benign probability of each vehicle evolves during defense, we set $n = 5$ and compute the complement of P_{benign} to obtain the malicious probability, as shown in Fig. 5. Since groups containing attackers are more likely to trigger abnormal detections, the normal detection count β_j of a malicious vehicle remains zero, causing its benign probability to vanish. Consequently, the malicious probabilities of all attackers rapidly reach 100%.

7. Conclusion

This paper tackles the challenge of defending against adversarial attacks in fully untrusted-vehicle CP by proposing the PRBI framework, which integrates adjacent-frame similarity analysis with pseudo-random Bayesian inference. By exploiting stability differences in perception results across adjacent frames, PRBI eliminates reliance on a trusted ego vehicle. It combines group-based validation and probabilistic inference to accurately identify malicious vehicles with only two additional verifications per frame. Theoretical analysis demonstrates the convergence of the estimated number of attackers, and comprehensive experiments further verify PRBI's significant advantages in defense efficiency and performance. These results highlight PRBI as an effective and resource-efficient defense for CP security in autonomous driving.

Acknowledgement. This work was supported by the National Natural Science Foundation of China (62441237, U24A20336), the Fundamental Research Funds for the Central Universities (2042025kf0055) and Wuhan City Joint Innovation Laboratory for Next-Generation Wireless Communication Industry Featuring Satellite-Terrestrial Integration under Grant 4050902040448.

References

- [1] Anique Akhtar, Zhu Li, and Geert Van der Auwera. Inter-frame compression for dynamic point cloud geometry coding. *IEEE Transactions on Image Processing*, 33:584–594, 2024. 2
- [2] Holger Caesar, Varun Bankiti, Alex H Lang, Sourabh Vora, Venice Erin Liong, Qiang Xu, Anush Krishnan, Yu Pan, Giancarlo Baldan, and Oscar Beijbom. nuscenes: A multi-modal dataset for autonomous driving. In *Proceedings of the IEEE/CVF Conference on Computer Vision and Pattern Recognition*, pages 11621–11631, 2020. 6
- [3] Yulong Cao, S Hrushikesh Bhupathiraju, Pirouz Naghavi, Takeshi Sugawara, Z Morley Mao, and Sara Rampazzi. You can’t see me: Physical removal attacks on {lidar-based} autonomous vehicles driving frameworks. In *Proceedings of 32nd USENIX Security Symposium*, pages 2993–3010, 2023. 1
- [4] Nicholas Carlini and David Wagner. Towards evaluating the robustness of neural networks. In *Proceedings of 2017 IEEE Symposium on Security and Privacy*, pages 39–57. IEEE, 2017. 6, 1
- [5] Zhengru Fang, Senkang Hu, Jingjing Wang, Yiqin Deng, Xianhao Chen, and Yuguang Fang. Prioritized information bottleneck theoretic framework with distributed online learning for edge video analytics. *IEEE Transactions on Networking*, 2025. 1
- [6] Xin Gao, Xinyu Zhang, Yiguo Lu, Yuning Huang, Lei Yang, Yijin Xiong, and Peng Liu. A survey of collaborative perception in intelligent vehicles at intersections. *IEEE Transactions on Intelligent Vehicles*, 2024. 1
- [7] R Spencer Hallyburton and Miroslav Pajic. Security-aware sensor fusion with mate: the multi-agent trust estimator. In *Proceedings of the 2025 ACM SIGSAC Conference on Computer and Communications Security*, pages 2009–2023, 2025. 2
- [8] Senkang Hu, Yihang Tao, Zihan Fang, Guowen Xu, Yiqin Deng, Sam Kwong, and Yuguang Fang. Cp-guard+: A new paradigm for malicious agent detection and defense in collaborative perception. *arXiv preprint arXiv:2502.07807*, 2025. 1, 2
- [9] Senkang Hu, Yihang Tao, Guowen Xu, Yiqin Deng, Xianhao Chen, Yuguang Fang, and Sam Kwong. Cp-guard: Malicious agent detection and defense in collaborative bird’s eye view perception. In *Proceedings of the AAAI Conference on Artificial Intelligence*, pages 23203–23211, 2025. 1, 2, 6, 7, 4
- [10] Yue Hu, Juntong Peng, Sifei Liu, Junhao Ge, Si Liu, and Siheng Chen. Communication-efficient collaborative perception via information filling with codebook. In *Proceedings of the IEEE/CVF Conference on Computer Vision and Pattern Recognition*, pages 15481–15490, 2024. 1
- [11] Zizhi Jin, Xiaoyu Ji, Yushi Cheng, Bo Yang, Chen Yan, and Wenyuan Xu. PLA-LIDAR: Physical laser attacks against lidar-based 3d object detection in autonomous vehicle. In *Proceedings of 2023 IEEE Symposium on Security and Privacy*, pages 1822–1839. IEEE, 2023. 1
- [12] Monish Keswani, Sriranjani Ramakrishnan, Nishant Reddy, and Vineeth N Balasubramanian. Proto2proto: Can you recognize the car, the way i do? In *Proceedings of the IEEE/CVF Conference on Computer Vision and Pattern Recognition*, pages 10233–10243, 2022. 4
- [13] Alexey Kurakin, Ian J Goodfellow, and Samy Bengio. Adversarial examples in the physical world. In *Artificial Intelligence Safety and Security*, pages 99–112. Chapman and Hall/CRC, 2018. 6, 1
- [14] Yiming Li, Shunli Ren, Pengxiang Wu, Siheng Chen, Chen Feng, and Wenjun Zhang. Learning distilled collaboration graph for multi-agent perception. *Advances in Neural Information Processing Systems*, 34:29541–29552, 2021. 6, 7, 4
- [15] Yiming Li, Dekun Ma, Ziyang An, Zixun Wang, Yiqi Zhong, Siheng Chen, and Chen Feng. V2x-sim: Multi-agent collaborative perception dataset and benchmark for autonomous driving. *IEEE Robotics and Automation Letters*, 7(4):10914–10921, 2022. 6, 1
- [16] Yiming Li, Qi Fang, Jiamu Bai, Siheng Chen, Felix Juefei-Xu, and Chen Feng. Among us: Adversarially robust collaborative perception by consensus. In *Proceedings of the IEEE/CVF International Conference on Computer Vision*, pages 186–195, 2023. 1, 2, 6, 7, 4
- [17] Yangfan Li, Mengquan Li, Cen Chen, Xiaofeng Zou, Honggen Shao, Fengxiao Tang, and Kenli Li. Simdiff: Point cloud acceleration by utilizing spatial similarity and differential execution. *IEEE Transactions on Computer-Aided Design of Integrated Circuits and Systems*, 2024. 2
- [18] Mingyu Liu, Ekim Yurtsever, Jonathan Fossaert, Xingcheng Zhou, Walter Zimmer, Yuning Cui, Bare Luka Zagar, and Alois C Knoll. A survey on autonomous driving datasets: Statistics, annotation quality, and a future outlook. *IEEE Transactions on Intelligent Vehicles*, 2024. 1
- [19] Yang Lou, Yi Zhu, Qun Song, Rui Tan, Chunming Qiao, Wei-Bin Lee, and Jianping Wang. A first {Physical-World} trajectory prediction attack via {LiDAR-induced} deceptions in autonomous driving. In *Proceedings of 33rd USENIX Security Symposium*, pages 6291–6308, 2024. 2
- [20] Wenjie Luo, Bin Yang, and Raquel Urtasun. Fast and furious: Real time end-to-end 3d detection, tracking and motion forecasting with a single convolutional net. In *Proceedings of the IEEE/CVF Conference on Computer Vision and Pattern Recognition*, pages 3569–3577, 2018. 6
- [21] Aleksander Madry, Aleksandar Makelov, Ludwig Schmidt, Dimitris Tsipras, and Adrian Vladu. Towards deep learning models resistant to adversarial attacks. *arXiv preprint arXiv:1706.06083*, 2017. 2, 6, 1
- [22] Suphakit Niwattanakul, Jatsada Singthongchai, Ekkachai Naenudorn, and Supachanun Wanapu. Using of jaccard coefficient for keywords similarity. In *Proceedings of the International Multiconference of Engineers and Computer Scientists*, pages 380–384, 2013. 2
- [23] Takami Sato, Ryo Suzuki, Yuki Hayakawa, Kazuma Ikeda, Ozora Sako, Rokuto Nagata, Ryo Yoshida, Qi Alfred Chen, and Kentaro Yoshioka. On the realism of lidar spoofing attacks against autonomous driving vehicle at high speed and long distance. In *Proceedings of the Network and Distributed System Security Symposium*, 2025. 1

- [24] Florian A Schiegg, Daniel Bischoff, Johannes R Krost, and Ignacio Llatser. Analytical performance evaluation of the collective perception service in IEEE 802.11 p networks. In *Proceedings of 2020 IEEE Wireless Communications and Networking Conference*, pages 1–6. IEEE, 2020. [2](#)
- [25] Yihang Tao, Senkang Hu, Yue Hu, Haonan An, Hangcheng Cao, and Yuguang Fang. Gcp: Guarded collaborative perception with spatial-temporal aware malicious agent detection. *arXiv preprint arXiv:2501.02450*, 2025. [1](#), [2](#)
- [26] Tzungyu Tsai, Kaichen Yang, Tsung-Yi Ho, and Yier Jin. Robust adversarial objects against deep learning models. In *Proceedings of the AAAI Conference on Artificial Intelligence*, pages 954–962, 2020. [2](#)
- [27] James Tu, Tsunhsuan Wang, Jingkang Wang, Sivabalan Manivasagam, Mengye Ren, and Raquel Urtasun. Adversarial attacks on multi-agent communication. In *Proceedings of the IEEE/CVF International Conference on Computer Vision*, pages 7768–7777, 2021. [1](#), [2](#), [3](#)
- [28] Chenyi Wang, Raymond Muller, Ruoyu Song, Jean-Philippe Monteuis, Jonathan Petit, Yanmao Man, Ryan Gerdes, Z Berkay Celik, and Ming Li. From threat to trust: Exploiting attention mechanisms for attacks and defenses in cooperative perception. In *34th USENIX Security Symposium*, pages 7387–7406, 2025. [2](#)
- [29] Tianhang Wang, Guang Chen, Kai Chen, Zhengfa Liu, Bo Zhang, Alois Knoll, and Changjun Jiang. Umc: A unified bandwidth-efficient and multi-resolution based collaborative perception framework. In *Proceedings of the IEEE/CVF International Conference on Computer Vision*, pages 8187–8196, 2023. [1](#)
- [30] Tsun-Hsuan Wang, Sivabalan Manivasagam, Ming Liang, Bin Yang, Wenyuan Zeng, and Raquel Urtasun. V2vnet: Vehicle-to-vehicle communication for joint perception and prediction. In *Proceedings of Computer Vision—ECCV 2020: 16th European conference, Glasgow, UK, August 23–28, 2020, proceedings, part II 16*, pages 605–621. Springer, 2020. [6](#), [7](#), [1](#)
- [31] Yubo Wang, Chaohu Liu, Yanqiu Qu, Haoyu Cao, Deqiang Jiang, and Linli Xu. Break the visual perception: Adversarial attacks targeting encoded visual tokens of large vision-language models. In *Proceedings of the 32nd ACM International Conference on Multimedia*, pages 1072–1081, 2024. [2](#)
- [32] Yizhou Wang, Libing Wu, Jiong Jin, Enshu Wang, Zhuangzhuang Zhang, and Yu Zhao. An imperceptible adversarial attack against 3d object detectors in autonomous driving. *IEEE Internet of Things Journal*, 2025. [2](#)
- [33] Chao Xiang, Chen Feng, Xiaopo Xie, Botian Shi, Hao Lu, Yisheng Lv, Mingchuan Yang, and Zhendong Niu. Multi-sensor fusion and cooperative perception for autonomous driving: A review. *IEEE Intelligent Transportation Systems Magazine*, 15(5):36–58, 2023. [6](#)
- [34] Yi Yu, Weizhen Han, Libing Wu, Bingyi Liu, Enshu Wang, and Zhuangzhuang Zhang. Enduring, efficient and robust trajectory prediction attack in autonomous driving via optimization-driven multi-frame perturbation framework. In *Proceedings of the Computer Vision and Pattern Recognition Conference*, pages 17229–17238, 2025. [2](#)
- [35] Qingzhao Zhang, Shuowei Jin, Ruiyang Zhu, Jiachen Sun, Xumiao Zhang, Qi Alfred Chen, and Z Morley Mao. On data fabrication in collaborative vehicular perception: Attacks and countermeasures. In *Proceedings of 33rd USENIX Security Symposium*, pages 6309–6326, 2024. [2](#)
- [36] Shenyi Zhang, Baolin Zheng, Peipei Jiang, Lingchen Zhao, Chao Shen, and Qian Wang. Perception-driven imperceptible adversarial attack against decision-based black-box models. *IEEE Transactions on Information Forensics and Security*, 19:3164–3177, 2024. [2](#)
- [37] Yangheng Zhao, Zhen Xiang, Sheng Yin, Xianghe Pang, Yanfeng Wang, and Siheng Chen. Made: Malicious agent detection for robust multi-agent collaborative perception. In *Proceedings of 2024 IEEE/RSJ International Conference on Intelligent Robots and Systems*, pages 13817–13823. IEEE, 2024. [1](#), [2](#), [3](#)

All Vehicles Can Lie: Efficient Adversarial Defense in Fully Untrusted-Vehicle Collaborative Perception via Pseudo-Random Bayesian Inference

Supplementary Material

8. Hypothesis Verification Experiments

To validate our assumption regarding the temporal stability of LiDAR-based perception, we conduct a dedicated hypothesis verification experiment using the V2X-Sim dataset [15] within the collaborative perception framework. Our goal is to examine whether perception outputs across consecutive frames maintain consistently high similarity under normal conditions, while experiencing a significant drop in similarity under adversarial perturbations.

Experimental Setup. We consider three representative types of driving scenes in V2X-Sim dataset: *urban*, *suburban*, and *intersection*, as shown in Fig. 7, where we provide representative LiDAR point cloud visualizations for each scene type. For each category, we randomly select 5–10 scenes, each containing multiple consecutive frames of multi-vehicle LiDAR data. Within each scene, we compute the Jaccard similarity between consecutive-frame detection outputs, using V2VNet [30] as the perception backbone. The evaluation is carried out for both:

- **Normal settings:**
 1. *Upper-Bound:* All vehicles are collaborative and benign.
 2. *Lower-Bound:* Only the ego vehicle’s own perception is used (*single-vehicle baseline*).
- **Adversarial settings:** All scenes re-evaluated under three widely used white-box attacks—BIM [13], C&W [4], and PGD [21]. Perturbations are injected into the feature maps of randomly selected malicious vehicles, following standard attack parameters.

Observations and Results. For Fig. 6, we visualize distribution statistics from *two randomly picked scenes (scene 4 & 78)* out of the entire test scenarios. This sub-selection is purely for clarity and readability of the plots; the trends are representative of the complete experimental results across all selected scenes. Fig. 6 clearly illustrates an evident separation between normal and adversarial regimes:

- Under **normal conditions** (both Upper- and Lower-Bound), inter-frame similarity consistently clusters around **0.8**, indicating strong temporal stability and spatial continuity of perception outputs.
- Under **adversarial attacks** (BIM, C&W, PGD), similarity values drop sharply, *often well below 0.3, and peaking only around 0.2*, reflecting the severe disruption of temporal consistency caused by injected perturbations.

These results hold across scene types and independent random samplings, confirming that the temporal stability signal is strong and scenario-agnostic.

Conclusion of Hypothesis Verification. The persistent and large margin between benign and adversarial similarity distributions validates our assumption: temporal similarity between successive LiDAR perception outputs is consistently high under benign conditions and substantially degraded under attack. This robust gap can serve as a reliable self-referential signal, forming a sound foundation for our proposed frame-wise self-supervision mechanism, without the need to assume a trusted ego vehicle.

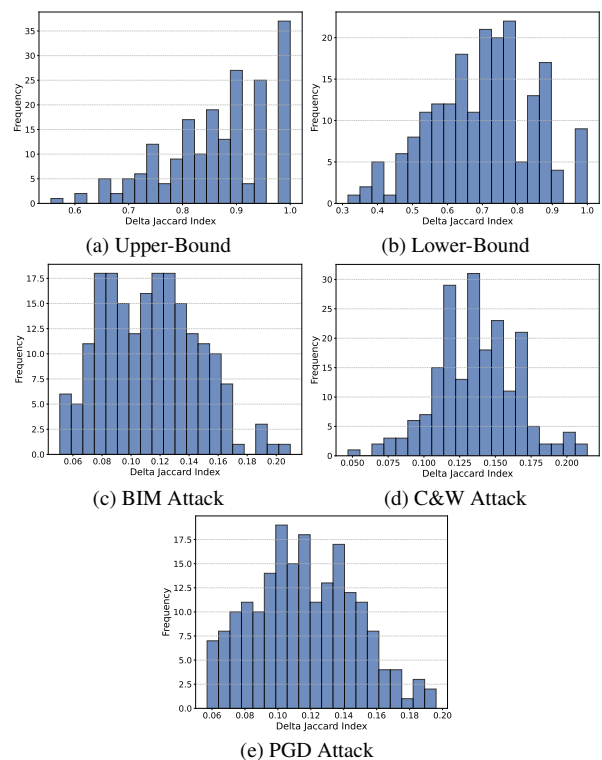


Figure 6. Hypothesis verification experiments. We report the Jaccard similarity of detected object sets between consecutive frames for: (a)-(b) normal conditions (Upper-Bound: all vehicles collaborate; Lower-Bound: ego-only perception), and (c)-(e) adversarial conditions (BIM, C&W, and PGD). Plots are based on statistics from two randomly selected representative scenes for readability; trends are consistent across all tested scenes and scenarios (urban, suburban, intersection).

9. The Pseudocode of PRBI Algorithm

In this section, we provide a detailed pseudocode of the proposed Pseudo-Random Bayesian Inference (PRBI) algo-

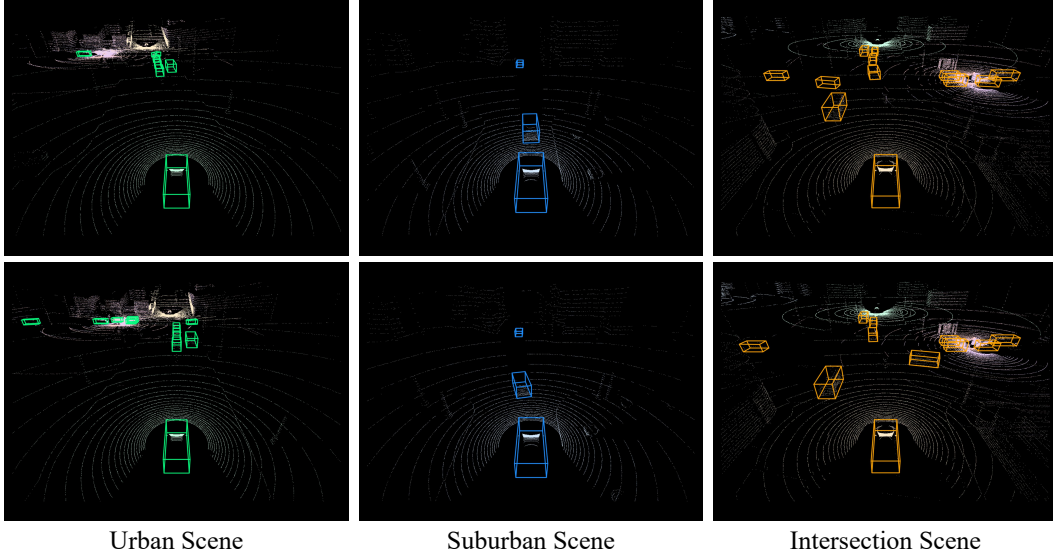


Figure 7. Example LiDAR point clouds illustrating three representative driving scenes in V2X-Sim dataset: urban, suburban, and intersection.

rithm. The PRBI framework is designed to detect malicious vehicles in collaborative perception with minimal verification attempts, thereby safeguarding the victim vehicle’s perception performance under adversarial conditions.

The full algorithm is outlined in Algorithm 1, which formalizes the PRBI defense mechanism for adversarial collaborative perception.

10. Theoretical Proof

10.1. Proof of Theorem 1

In **Soft Sampling**, we adopt a pseudo-random grouping strategy that assigns the top $\lfloor m \rfloor$ most suspicious vehicles into one group, and the remaining vehicles into the second group. A key question naturally arises — **Can m converge to the true number of attackers k ?** This subsection presents a proof showing why pseudo-random grouping ensures that m will indeed converge to the true attacker count k .

Assume the estimated number of attackers at frame i is m . We aim to prove that the estimate at the next frame, m' , will move toward k . The proof is divided into two parts:

(1) When $m < k$, then m' will increase: According to the definition of soft sampling, at frame $i + 1$, the grouping consists of “ m suspicious vehicles + $(n - m)$ remaining vehicles”. Since $m < k$, there must still be at least one attacker in the remaining group. As a result, the normal detection count β for both groups will not increase and remains unchanged. The new estimate m' is:

$$m' = \log_2 \left(\frac{n \cdot (N + 1)}{\sum \beta} \right) > \log_2 \left(\frac{n \cdot N}{\sum \beta} \right) = m. \quad (15)$$

Thus, part (1) is proven based on Eq. (15).

(2) When $m \geq k$, then m' will decrease: Again, the frame $i + 1$ grouping consists of “ m suspicious vehicles + $(n - m)$ remaining vehicles”. However, this time, the remaining group contains no attackers. The normal detection count for the first group remains unchanged, while the second group contributes $n - m$ additional normal detections. The updated estimate becomes:

$$m' = \log_2 \left(\frac{n \cdot (N + 1)}{n - m + \sum \beta} \right). \quad (16)$$

To prove part (2), we must prove the next inequality:

$$m' = \log_2 \left(\frac{n \cdot (N + 1)}{n - m + \sum \beta} \right) < \log_2 \left(\frac{n \cdot (N)}{\sum \beta} \right) = m. \quad (17)$$

Removing the logarithm and rewriting the right-hand side using 2^m , the Eq. (17) becomes:

$$\frac{n \cdot (N + 1)}{n - m + \sum \beta} < 2^m. \quad (18)$$

Divide by $\sum \beta$ to get:

$$\frac{2^m + n / \sum \beta}{1 + (n - m) / \sum \beta} < 2^m. \quad (19)$$

Simplifying further and rearranging terms, the goal is to prove:

$$m + \frac{m}{2^m - 1} < n. \quad (20)$$

Define $f(m) = m + \frac{m}{2^m - 1}$ for $m \in [1, n - 1]$. Taking the derivative of $f(m)$ and we can easily know that $f(m)$ is

Algorithm 1 Pseudo-Random Bayesian Inference

Input: Number of CAVs n ; Detection count arrays $\mathbf{c}_{\text{normal}}$, $\mathbf{c}_{\text{abnormal}}$; Similarity threshold ϵ ; Hypothesis testing window size w .

Output: Malicious vehicles: $\text{Attackers} = \{id_1, \dots, id_k\}$

```

1:  $\mathbf{c}_{\text{normal}} \leftarrow \mathbf{0}$ ,  $\mathbf{c}_{\text{abnormal}} \leftarrow \mathbf{0}$ ,  $N \leftarrow 0$ 
2:  $m \leftarrow n - 1$ ,  $P_{\text{benign}} \leftarrow \mathbf{0}$ 
3:  $W \leftarrow \text{Queue}()$ ,  $\text{convergence} \leftarrow \text{False}$ 
4: while system running,  $i \leftarrow i + 1$  do
5:    $D_1^i \leftarrow \text{Perception}(F_1^i, \dots, F_n^i)$ 
6:   if  $i = 0$  then
7:      $D_{\text{ref}} \leftarrow D_1^i$   $\triangleright$  Initialize reference frame
8:      $D_1^i$  as PerceptionOutput
9:     continue
10:  end if
11:  if  $\text{Jaccard}(D_1^i, D_{\text{ref}}) < \epsilon$  and  $\text{convergence} = \text{False}$  then
12:     $\triangleright$  Soft Sampling
13:     $\text{Group}_1 \leftarrow \text{argsort}(P_{\text{benign}})_{0:\lfloor m \rfloor}$ 
14:     $\text{Group}_2 \leftarrow \text{argsort}(P_{\text{benign}})_{\lfloor m \rfloor:n}$ 
15:     $\triangleright$  Consistency Validation
16:     $D_{\text{Group}_{1,2}} \leftarrow \text{Perception}(\text{Group}_{1,2})$ 
17:    Compare  $\text{Jaccard}(D_{\text{Group}_{1,2}}, D_{\text{ref}})$  with  $\epsilon$ 
18:    Update  $\mathbf{c}_{\text{normal}}$ ,  $N$ , and  $\mathbf{c}_{\text{abnormal}}$ 
19:     $\triangleright$  Attacker Evaluation
20:     $m \leftarrow \min\left(\log_2\left(\frac{n \cdot N}{\sum(\mathbf{c}_{\text{normal}})}\right), n - 1\right)$ 
21:    for  $id = 1$  to  $n$  do
22:       $P_{\text{benign}}[id] \leftarrow \text{Bayesian}(\mathbf{c}_{\text{nor}}, \mathbf{c}_{\text{abnor}}, N)$ 
23:    end for
24:     $\text{Attackers} \leftarrow \text{argsort}(P_{\text{benign}})_{0:\lfloor m \rfloor}$ 
25:     $\triangleright$  Hypothesis Test
26:     $W.\text{push}(m)$  with size limit  $w$ 
27:    if T-test( $W$ ) indicates convergence then
28:       $\text{convergence} \leftarrow \text{True}$ 
29:      Output  $\text{Attackers}$ 
30:    else
31:       $\text{Collaborators} \leftarrow \{i \mid P_{\text{benign}}[i] \neq 0\}$ 
32:      if  $\text{Collaborators} = \emptyset$  and first abnormal
frame then
33:         $\text{Collaborators} \leftarrow$  first valid subset
from recursive split of  $\text{Group}_{1,2}$ 
34:        Update  $\mathbf{c}_{\text{normal}}$ ,  $N$ , and  $\mathbf{c}_{\text{abnormal}}$ 
35:      end if
36:       $D_1^i \leftarrow \text{Perception}(\text{Collaborators})$ 
37:       $D_{\text{ref}} \leftarrow D_1^i$ 
38:       $D_1^i$  as PerceptionOutput
39:    end if
40:  else
41:    Collaborative perception excluding  $\text{Attackers}$ 
42:  end if
43: end while

```

increasing for $m \in [1, n - 1]$. Thus, we have:

$$f(m) \leq f(n - 1) = n + \frac{2n - 2^n}{2^n - 2}. \quad (21)$$

When $n = 2$, m can only be 1. In this special case, equality holds, and m' always stays at 1. When $n > 2$, since $2n - 2^n < 0$, we have:

$$f(m) \leq n + \frac{2n - 2^n}{2^n - 2} < n. \quad (22)$$

Based on Eq. (22), the Eq. (20) holds and part (2) is proven.

10.2. Proof of Theorem 2

In Sec. 10.1, we have proven that under the pseudo-random grouping strategy, the estimated number of attackers m will always converge toward the true number of attackers k . In practical applications, it is essential to address another important issue — *How should m be rounded?* Since m tends to converge to k , directly applying standard rounding (i.e., rounding to the nearest integer) when evaluating suspicious malicious vehicles may suffice. However, during the **pseudo-random grouping** process, m may not yet have fully converged, and different rounding strategies can influence the convergence outcome. We now provide a detailed derivation of these effects under the same settings and leveraging the proven proof (1), (2) in Sec. 10.1:

(a) Rounding to the nearest integer $\lfloor m \rfloor$: When $m \in (-\infty, k - 0.5)$, we have $\lfloor m \rfloor < k$. According to proof (1), the next frame's m' will increase. When $m \in [k - 0.5, +\infty)$, $\lfloor m \rfloor \geq k$, and m' will decrease based on proof (2). Therefore, m ultimately converges to approximately $k - 0.5$. The subsequent derivations are carried out in the same way.

(b) Ceiling $\lceil m \rceil$: When $m \in (-\infty, k - 1)$, we have $\lceil m \rceil < k$, and m' will increase. When $m \in [k - 1, +\infty)$, $\lceil m \rceil \geq k$, and m' will decrease. Thus, m ultimately converges to approximately $k - 1$. Note that when the true number of attackers $k = 1$, m will not tend toward 0, because the argument of a logarithm in Eq. (15) can never be one. In this case, apart from the malicious vehicle, each of the remaining $(n - 1)$ benign vehicles undergoes one successful normal detection per frame. Thus, the final m is:

$$m \cong \log_2\left(\frac{n \cdot N}{(n - 1) \cdot N}\right) = \log_2\left(\frac{n}{n - 1}\right). \quad (23)$$

(c) Floor $\lfloor m \rfloor$: When $m \in (-\infty, k)$, we have $\lfloor m \rfloor < k$, and m' will increase. When $m \in [k, +\infty)$, $\lfloor m \rfloor \geq k$, and m' will decrease. Hence, m ultimately converges to k .

In conclusion, **only by applying floor rounding ($\lfloor m \rfloor$) in the pseudo-random grouping strategy can we ensure that m converges to k .**

11. Experimental Results

11.1. Experimental Details

Adversarial Optimization. Perturbations are added to all malicious vehicles’ features and optimized jointly. For adversarial attacks, the step size is set to 0.1, the perturbation stealth metric to 0.3, and the number of iterations to 15.

Baselines and Implementation. We randomly select 5 scenarios from the V2X-Sim test set, each consisting of 100 frames. Collaborative perception scenarios involve 6 collaborators (1 RSU and 5 vehicles, with the first vehicle being the ego/victim). Detection model training follows the default setup in DiscoNet [14]. For baseline defenses, ROBOSAC [16] strictly follows the official configuration and always selects the maximum possible number of collaborators for joint perception to ensure fairness and stability. PASAC [9] also adopts its official hyperparameter settings for the consistency loss module. All baseline implementations are reproduced under the same perception backbone, communication setup, and attack conditions for a fair comparison.

Defense Hyperparameters. The Jaccard similarity threshold ϵ is 0.35, the verification window size w is 10, the confidence level α for the T-test is 0.01, and the probability weights γ and λ are set to 0.35 and 0.65, respectively. The setting of the similarity threshold is based on the following considerations: (1) a relatively large threshold may occasionally misclassify benign vehicles as malicious in a single frame, but such errors can be corrected in subsequent frames; (2) setting the threshold too small risks misclassifying malicious vehicles as benign, yet this is tolerable in our framework. Specifically, a false negative occurs when malicious vehicles exhibit high similarity, implying that the attack has not significantly impacted perception and thus does not cause irreversible consequences. Conversely, effective attacks induce a sustained drop in similarity, and our probabilistic updating mechanism ensures that such malicious vehicles will eventually be identified. Combined with the experimental results in Sec. 8 (where adversarial cases rarely exceed 0.3), we adopt 0.35 as a balanced threshold.

11.2. Varying Test Parameters

In the scenario where the total number of vehicles is set to 5, the results of the hypothesis testing parameter (α and w) experiments for all attacker ratios are presented in Tab. 5. We document the total number of frames required to achieve convergence under each setting (**Average Converge Frames**), the identification rate of malicious vehicles upon convergence (**Identification Rate**), and the misclassification rate of benign vehicles upon convergence (**Misclassification Rate**). The results show that regardless of the proportion of attackers, the convergence speed is always inversely proportional to the confidence level α and directly

Table 5. Comprehensive experimental results of different test parameters on defense effect. *ID Rate*: malicious vehicle identification rate. *MC Rate*: benign vehicle misclassification rate.

Settings	Count		Avg. Count		Avg. Frames	ID Rate	MC Rate
	Min	Max	Min	Max			
Confidence Level (20% Attackers)							
Conf. 0.20	2	2	2.00	2.00	2.00	2.53	100% 0%
Conf. 0.15	2	2	2.00	2.00	2.00	2.27	100% 0%
Conf. 0.10	2	2	2.00	2.00	2.00	2.29	100% 0%
Conf. 0.05	2	2	2.00	2.00	2.00	2.19	100% 0%
Conf. 0.01	2	2	2.00	2.00	2.00	2.25	100% 0%
Confidence Level (40% Attackers)							
Conf. 0.20	2	4	2.00	3.02	2.38	3.13	100% 9%
Conf. 0.15	2	4	2.00	3.00	2.37	3.04	100% 8%
Conf. 0.10	2	4	2.00	2.96	2.35	2.98	100% 8%
Conf. 0.05	2	4	2.00	2.91	2.34	2.77	100% 4%
Conf. 0.01	2	4	2.00	2.88	2.35	2.77	100% 6%
Confidence Level (60% Attackers)							
Conf. 0.20	2	6	2.00	4.22	2.61	3.99	100% 0%
Conf. 0.15	2	6	2.00	4.12	2.62	3.51	100% 0%
Conf. 0.10	2	6	2.00	3.94	2.53	3.44	100% 0%
Conf. 0.05	2	6	2.00	4.26	2.67	3.40	100% 0%
Conf. 0.01	2	6	2.00	4.06	2.61	3.36	100% 0%
Confidence Level (80% Attackers)							
Conf. 0.20	2	8	2.00	6.06	2.50	10.01	100% 0%
Conf. 0.15	2	8	2.00	5.86	2.51	9.31	100% 0%
Conf. 0.10	2	8	2.00	6.24	2.80	6.58	100% 0%
Conf. 0.05	2	8	2.00	6.04	2.77	6.51	100% 0%
Conf. 0.01	2	8	2.00	5.70	2.86	4.27	100% 0%
Window Size (20% Attackers)							
Size 10	2	2	2.00	2.00	2.00	2.25	100% 0%
Size 8	2	2	2.00	2.00	2.00	2.37	100% 0%
Size 6	2	2	2.00	2.00	2.00	2.35	100% 0%
Size 4	2	2	2.00	2.00	2.00	2.33	100% 0%
Window Size (40% Attackers)							
Size 10	2	4	2.00	2.88	2.35	2.77	100% 6%
Size 8	2	4	2.00	3.12	2.46	2.80	100% 7%
Size 6	2	4	2.00	3.00	2.39	2.84	100% 4%
Size 4	2	4	2.00	3.02	2.40	2.94	100% 11%
Window Size (60% Attackers)							
Size 10	2	6	2.00	4.06	2.61	3.36	100% 0%
Size 8	2	6	2.00	4.08	2.62	3.33	100% 0%
Size 6	2	6	2.00	4.32	2.69	3.34	100% 0%
Size 4	2	6	2.00	4.14	2.63	3.41	100% 0%
Window Size (80% Attackers)							
Size 10	2	8	2.00	5.70	2.86	4.27	100% 0%
Size 8	2	8	2.00	6.16	2.91	4.60	100% 0%
Size 6	2	8	2.00	6.10	2.89	4.57	100% 0%
Size 4	2	8	2.00	6.34	2.88	4.89	100% 0%

proportional to the window size w . For instance, when the α is set to 0.2, the average maximum number of frames required for convergence is 10.01 frames; while the α is

Table 6. Defense performance under intermittent attacks.

Methods	V2VNet		DiscoNet	
	AP@0.5 / 0.7	ID / MC	AP@0.5 / 0.7	ID / MC
1 frame	68.91 / 65.57	100% / 0%	69.37 / 65.89	100% / 0%
3 frames	70.97 / 65.91	100% / 0%	69.12 / 66.27	100% / 0%
5 frames	73.52 / 67.04	100% / 0%	70.43 / 66.91	100% / 0%

reduced to 0.01, the average minimum number of frames needed for convergence is only 2.25 frames. Additionally, the experimental results show that under all test conditions, the identification rate of malicious vehicles reaches 100%, fully verifying the high robustness of the proposed method.

11.3. Robustness to Intermittent Attacks

We further evaluate PRBI under intermittent attacks, where adversarial perturbations are injected periodically every 1, 3, or 5 frames. The total number of vehicles is set to $n = 5$, and all other experimental settings remain consistent with the main text.

PRBI is inherently robust to intermittent attacks due to its temporal Bayesian updating mechanism. Even when attacks occur sporadically, the posterior benign probability of malicious vehicles decreases cumulatively over time, leading to their progressive exclusion from the collaborator subset. As shown in Tab. 6, PRBI consistently achieves 100% attacker identification with 0% benign misclassification under all attack frequencies. Detection performance remains stable across both V2VNet and DiscoNet backbones, demonstrating strong robustness against temporally sparse adversarial behavior.

11.4. Sensitivity Analysis of Similarity Threshold ϵ

We evaluate the sensitivity of PRBI to the similarity threshold ϵ under standard adversarial settings. The total number of vehicles is set to $n = 5$, and other experimental configurations remain consistent with the main text.

As shown in Tab. 7, PRBI maintains 100% attacker identification and 0% benign misclassification across a wide range of thresholds $\epsilon \in [0.30, 0.50]$. This indicates that the correctness of PRBI does not critically depend on precise threshold tuning. From a performance perspective, smaller ϵ values lead to slightly faster convergence but may introduce marginal reductions in detection precision, whereas larger ϵ values enforce stricter consistency validation, resulting in improved stability at the cost of modestly increased convergence latency. This behavior reflects a controllable strictness–efficiency trade-off.

Overall, the robustness of PRBI primarily stems from its probabilistic temporal accumulation mechanism rather than the specific value of ϵ . Empirically, $\epsilon = 0.35$ achieves the best balance between detection accuracy and convergence speed.

Table 7. Sensitivity of PRBI to similarity threshold ϵ under standard adversarial settings.

ϵ	AP@0.5 / 0.7	Avg. Convergence Frames
0.30	69.17 / 64.14	2.41
0.35	69.44 / 66.00	2.74
0.40	68.61 / 64.14	2.90
0.45	69.40 / 65.80	2.93
0.50	67.47 / 64.96	2.88

ID Rate: 100%, MC Rate: 0% across all settings